

PERFORMANCE TRADE-OFFS AND DESIGN LIMITATIONS OF ANALOG-TO-INFORMATION CONVERTER FRONT-ENDS

Omid Abari, Fred Chen, Fabian Lim and Vladimir Stojanović

Department of EECS, Massachusetts Institute of Technology, Cambridge, MA 02139, USA

ABSTRACT

This paper evaluates the impact of circuit impairments on the energy cost and performance limitations of analog-to-information converters (AIC). In applications where signal frequencies are high, but information bandwidths are low, AICs have been proposed as a potential solution to overcome the resolution and performance limitations of sampling jitter in high-speed analog-to-digital converters (ADC). Although the AIC architecture facilitates slower ADCs, the signal encoding, typically realized with a mixer-like circuit, still occurs at the Nyquist frequency of the input to avoid aliasing. We show that the jitter of this mixing stage limits the achievable AIC resolution. In this work, the end-to-end system evaluation framework is designed to analyze these limitations as well as the relative energy-efficiency of AICs versus ADCs across the resolution, receiver gain and signal sparsity. The evaluation shows that AICs improve the resolution by 1 bit when the signal of interest is very sparse, and enable 2x in energy savings when no pre-amplification is required.

Index Terms— Analog-to-information converter (AIC), compressed sensing (CS), analog-to-digital converter (ADC)

1. INTRODUCTION

Cognitive radio has been proposed as an intelligent wireless communication system to improve the utilization of the available bandwidth [1]. In such a system, it is required to simultaneously observe the entire frequency spectrum to determine the location of used channels. A straightforward approach is to monitor the spectrum range of interest by simply utilizing a wideband, Nyquist rate high speed analog-to-digital converter (ADC). A severe drawback is that ADCs working at such high frequencies (10's of GS/s) require high power and have limited resolution [2], [3]. An alternative approach is to utilize an analog-to-information converter (AIC) based on compressed sensing (CS) techniques [4]. CS is a promising method for recovering sparse signals from fewer measurements than ordinarily used in Shannon's sampling theorem [5]. Consequently, AICs can relax the frequency requirements of ADCs, potentially enabling higher resolution and/or lower power receiver front-ends.

In this work, we analyze the energy/performance design space of AICs in an example cognitive radio environment with 1000 channels that span the 500MHz-20GHz frequency spectrum. In particular, we explore how jitter, which commonly limits ADC performance at high sampling rates, impacts the performance of the AIC system. As we will show, AICs can enable higher effective number of bits (ENOB) than Nyquist-rate ADCs for signals with low sparsity level, but may require higher power. This depends on the nature of the input signal and some other factors such as signal sparsity and the required amplifier gain.

The remainder of the paper is as follows. Section 2 begins with a brief introduction to CS theory. Section 3 provides power models for implementation of AIC and high speed ADC systems. The mixer clocking jitter model is provided in Section 4. In Section 5, we describe the CS reconstruction and system evaluation framework that incorporates the noise and power models. Finally, Section 6 illustrates the energy and performance evaluation results.

2. COMPRESSED SENSING BACKGROUND

Signals are represented with varying levels of sparsity in different domains. For example, a single tone sine wave is either represented by a single frequency coefficient, or an infinite number of time-domain samples. Consider signals f represented as follows

$$f = \Psi x, \quad (1)$$

where x is the coefficient vector for f , which is expanded in the basis $\Psi \in \mathbb{R}^{N \times N}$. When a signal is sparse most of its coefficients are zero, or they are small enough to be ignored without much perceptual loss.

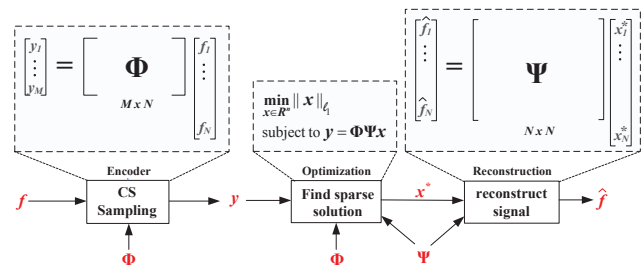


Figure 1: Compressed sensing (CS) framework.

The CS framework is shown in Fig. 1, where an N -dimensional input signal \mathbf{f} is compressed to M measurements \mathbf{y} , by taking M linear random projections, i.e.

$$\mathbf{y} = \Phi \mathbf{f}, \quad (2)$$

where $\Phi \in \mathbb{R}^{M \times N}$, $\mathbf{f} \in \mathbb{R}^{N \times 1}$ and $M < N$. In this case the system is undetermined, which means there are infinite number of solutions for \mathbf{f} . However, the signal is known *a-priori* to be sparse. Under certain conditions, the sparsest signal representation satisfying (2) can be shown to be unique.

Furthermore, solving the following convex program

$$\min_{\mathbf{x} \in \mathbb{R}^N} \|\mathbf{x}\|_{l_1} \text{ subject to } \mathbf{y} = \Phi \Psi \mathbf{x}, \quad (3)$$

can be shown to produce the sparsest solution [5].

3. SIGNAL AND POWER MODELS

In this section, we provide power models used to evaluate the energy cost of both the high-speed ADC system and an implementation of the AIC system. The signal model

$$f(t) = \sum_{j=1}^N x_j \sin(\omega_j t) \quad (4)$$

consists of user information coefficients, x_j , riding on the carriers, ω_j (in the range of 500MHz-20GHz), and emulates sparse narrowband or banded OFDM communication channels. Our sparsity assumption states that only $S \ll N$ coefficients, x_j , are non-zero, i.e. only S users are “active” at any one time. Figure 2(a) shows the block diagram of a typical AIC implementation [4]. In this architecture, the input signal $f(t)$ is amplified by M amplifiers. Each signal branch is then individually mixed by a different pseudorandom number (PN) waveform $\Phi_i(t)$ to perform CS-type random sampling. The mixer output is then integrated over a window of N Nyquist-rate sampling periods. Finally, the integrator outputs are sampled, quantized, and used to reconstruct the input signal. Figure 2(b) shows the same functionality implemented simply using an amplifier and an ADC operating at Nyquist-rate (with sampling rate N times that of ADCs in Fig. 2(a)).

The potential advantages of using AICs in this context stem from having a different sensitivity to sources of jitter introduced by different control signals in the AIC system.

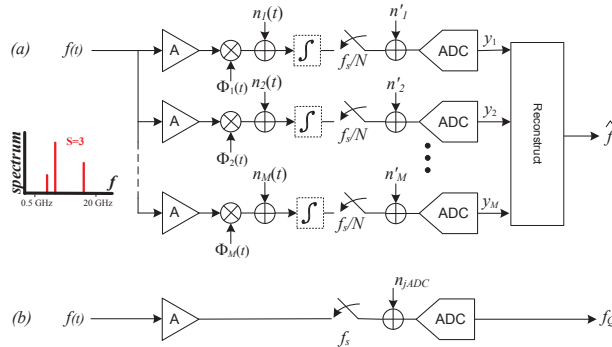


Figure 2: Block diagram of (a) an AIC system, and (b) a high-speed ADC system both with same functionality in the cognitive radio setting.

In the AIC system in Fig. 2(a), the jitter error from sampling clocks on the slower ADCs is negligible, whereas the main source of error comes from the jitter in the PN waveform mixed with the input signal at the Nyquist frequency. In a Nyquist-rate ADC, Fig. 2(b), the main noise source is due to sampling jitter in the high-speed ADC clock. In the following, we explain the energy models adopted for the two systems.

3.1. AIC System Power

As described in [6], the total power, P_{AIC} , of the AIC system in Fig. 2(a) can be summarized as

$$P_{AIC} = 2BW_f \left[\underbrace{\frac{M}{N} \cdot FOM \cdot 2^{ENOB}}_{ADCs} + \underbrace{\frac{M \cdot V_{DDA}^2 \cdot 10\pi \cdot N \cdot C_p}{16}}_{integrators} + \underbrace{\frac{3M \cdot N \cdot 2^{2 \cdot ENOB} \cdot G_A^2 (NEF)^2 \cdot \pi (k \cdot T)^2}{V_{DDA} \cdot q}}_{amplifiers} \right], \quad (5)$$

where the following quantities, process dependent capacitance (C_p), absolute temperature (T), Boltzmann constant (k), elementary charge (q), signal bandwidth (BW_f), amplifier noise efficiency factor (NEF), and ADC figure of merit (FOM), are all fixed parameters. The tunable parameters for the AIC system will be N , M , $ENOB$, and amplifier gain G_A . Note that we set $NEF=3$ and $FOM=100$ fJ/conversion step, consistent with the general performance of state of the art low-noise amplifiers and moderate-rate ADCs [6].

3.2. High Speed ADC System Power

As described in [6], the total power of the high-speed ADC system can be summarized as

$$P_{ADC} = 2BW_f \cdot \left[\underbrace{FOM \cdot 2^{ENOB}}_{ADC} + \underbrace{12 \cdot 2^{2 \cdot ENOB} \cdot \frac{G_A^2 (NEF)^2 \cdot \pi (k \cdot T)^2}{V_{DDA} \cdot q}}_{amplifier} \right], \quad (6)$$

with the same constants defined in (5). For this evaluation, $ENOB$ is the only tunable parameter for the ADC system, while $FOMs$ of 0.5, 1 and 5 pJ/conversion step are used to represent a range of possible efficiencies for high-speed ADC designs.

4. MIXER CLOCKING JITTER

Figure 3 shows our jitter noise model where the noise is multiplied by the input signal and filtered in the integrator block. The i -th PN waveform $\Phi_i(t)$ satisfies:

$$\Phi_i(t) = \sum_{j=1}^N \phi_{ij} p(t - jT_s) \quad (7)$$

where ϕ_{ij} is the (i,j) -th PN element, and $p(t)$ is a unit height pulse supported on $-T_s/2$ to $T_s/2$. Denoting the jittered PN

waveform as $\hat{\Phi}_i(t)$, then: $\hat{\Phi}_i(t) = \Phi_i(t) + N_i(t)$. Here, $N_i(t)$ is the jitter noise affecting $\hat{\Phi}_i(t)$, described as :

$$N_i(t) = \sum_{j=1}^{N+1} (\phi_{j-1} - \phi_j) \text{sgn}(\varepsilon_j) p'_j(t - jT_s + T_s/2), \quad (8)$$

where the jitter width is $\varepsilon \sim N(0, \sigma)$ with σ equal to the jitter rms, and $p'_j(t)$ is a unit amplitude pulse supported over the interval $[\min(0, \varepsilon_j), \max(0, \varepsilon_j)]$. In our model for $N_i(t)$, the process ε is the same for all PN waveforms, because we assume the same PLL is used across all measurements. Therefore the model captures this spatial correlation.

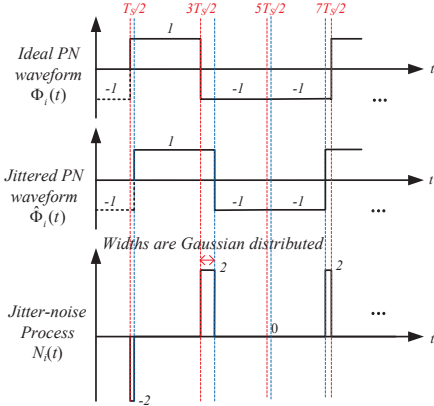


Figure 3: Ideal and jittered PN waveforms

5. RECONSTRUCTION FRAMEWORK

We now frame the reconstruction problem for the AIC within the CS framework described in Section 2. As shown in Fig. 2(a), each measurement, y_i , is computed by integrating the sum of noise, $n_i(t) = f(t) \cdot N_i(t)$, and the product of the signal, $f(t)$, and PN waveform, $\Phi_i(t)$:

$$y_i = \int_{T_s/2}^{N \cdot T_s + T_s/2} f(t) \cdot \Phi_i(t) dt + \int_{T_s/2}^{N \cdot T_s + T_s/2} n_i(t) dt. \quad (9)$$

Substituting the signal model from (4), the measurements are $\mathbf{y} = \Phi \Psi \mathbf{x} + \mathbf{n}^o$, where PN matrix Φ has entries ϕ_{ij} and

$$\Psi_{ij} = \int_{(i-1)T_s + T_s/2}^{iT_s + T_s/2} \sin(\omega_j t) dt, \quad \text{and} \\ n_i^o = \int_{T_s/2}^{N \cdot T_s + T_s/2} n_i(t) dt = \int_{T_s/2}^{N \cdot T_s + T_s/2} f(t) \cdot N_i(t) dt \quad (10)$$

where $\mathbf{n}^o = (n_1^o, n_2^o, \dots, n_M^o)^T$. Here, the jitter-induced noise n_i^o is merely the projection of $f(t)$ by the i -th jitter noise pulse process $N_i(t)$ (see Fig. 3).

6. EVALUATION RESULTS

In our signal model (4), we assume $N=1000$ possible subcarriers, and draw the S non-zero coefficient values, x_i ,

from a uniform random source. To compare the performance of the ADC and AIC systems, we adopt the same ENOB metric from ADC literature, which can be defined as:

$$\text{ENOB} = \log_2 \left(\frac{V_{\text{swing}}}{|\mathbf{f} - \hat{\mathbf{f}}| \cdot \sqrt{12}} \right) \quad (11)$$

where V_{swing} is the full-scale input voltage range of the ADCs and $|\mathbf{f} - \hat{\mathbf{f}}|$ is the rms signal distortion (use f_Q in place of \hat{f} for the Nyquist-rate ADC in Fig. 2(b)). We next analyze the energy-efficiency of the two systems using (5) and (6).

6.1 Jitter-limited ENOB

The jitter-limited ENOB for both systems is plotted in Fig. 4. As sparsity level S increases, the ENOB performance of the AIC system worsens while the high-speed ADC system improves. The reasons for this are as follows. In the receiver, the input signal $f(t)$ peaks are always normalized to V_{swing} , the full-scale voltage range of the ADC. When S increases, this normalization causes the coefficient values $|x_j|$ to get smaller with respect to V_{swing} . In ADCs, the jitter-error is dominated by the highest input frequencies, i.e. $|f - \hat{f}_Q| \approx |x_j \sin(\omega_j t) - x_j \sin(\omega_j t + \tau(t))|$ where $\tau(t)$ is the timing error caused by the jitter and ω_j is large. The ENOB increases since $V_{\text{swing}}/|f - \hat{f}_Q|$ increases with S (11). On the other hand, the

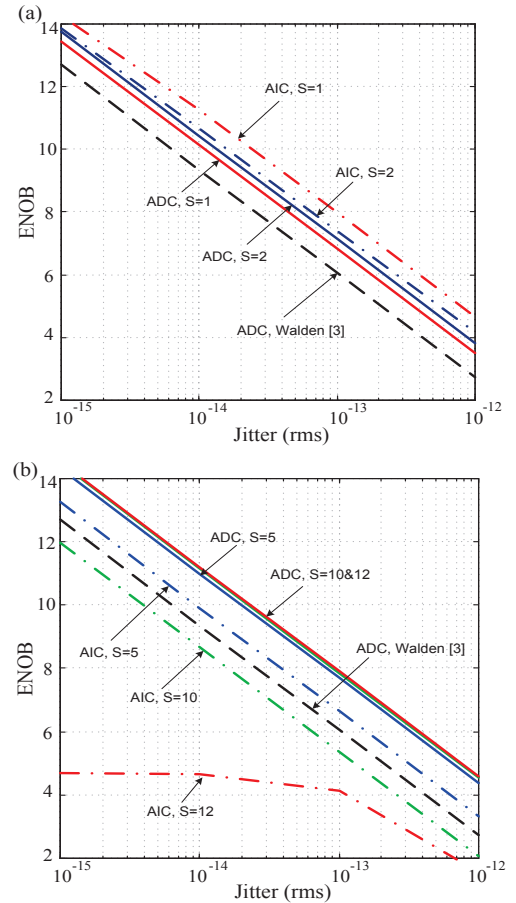


Figure 4: Jitter (rms) versus ENOB for signal sparsity of (a) $S = 1, 2$, and (b) $S = 5, 10, 12$, ($M = 100$ for all S).

AIC system has a different behavior. As S increases, AIC distortion $|f - \hat{f}|$ gets worse, resulting in poorer ENOB performance.

As shown in Fig. 4, the AIC system can improve the ENOB by 1 and 0.25 bits for a signal sparseness of 1 and 2, respectively. For signals with higher sparsity level S , the Nyquist ADC performs better than the AIC. Figure 4 also shows that compared to a standard Walden curve [3], in practice, the Nyquist ADC can achieve a better resolution because the input signal, $f(t)$, does not always consist of the highest frequency in the available signal bandwidth.

6.1 ENOB vs. Power

The AIC system power, $P_{AIC}(5)$, is a function of the ENOB, M and amplifier gain G_A . Figure 5 plots the power curves of both AIC and ADC systems vs. ENOB, for different M with $G_A=1$. The AIC power flattens for ENOBs less than 9 since the power is dominated by the integrator power, which is independent of ENOB. For higher resolutions, the amplifier power, which is an exponential function of ENOB, becomes dominant in the AIC system. Figure 5 also shows that increasing M increases the AIC power as the number of components scale with the number of measurements. However, increasing M also improves the CS reconstruction, which results in higher ENOB in the AIC system. For example, when $M = 100$, an ENOB of 5-12 is achievable for input signals with sparsity level equal to or less than 11. Finally, note that the grayed areas in the plots show impractical regions due to chip thermal limits.

As mentioned earlier, the total receiver gain must be set such that the input range of the ADC is accommodated. Hence, in addition to M , the amplifier gain G_A is also considered to evaluate the energy efficiency of the AIC and Nyquist ADC systems. Figure 6 shows the power of both systems vs. ENOB for different values of G_A when $M=100$. The AIC power increases due to an increase in amplifier power with G_A . However, the Nyquist ADC power changes very little since the power of the single amplifier is not dominant. In general, the AIC system has lower energy cost only for applications that require low amplifier gain.

7. CONCLUSION

In this work, we compared the energy cost and performance limitations of AIC and Nyquist ADC systems in the context of cognitive radio applications where the input signal is sparse in the frequency domain. Although AICs have been proposed as a potential solution to overcome the resolution and performance limitations of sampling jitter in high-speed Nyquist ADCs, the jitter in the mixer stage of AICs, which also works at the Nyquist rate, is found to similarly limit the resolution of AICs. However, for applications where low amplifier gain is acceptable and the input signal is very sparse, AICs have the potential to improve resolution and enable roughly a 2x reduction in power.

8. ACKNOWLEDGEMENT

This work was supported in part by the NSF award ECCS-1128226 and the National Science and Engineering Research Council of Canada (NSERC).

9. REFERENCES

- [1] Mitola, III, J. "Cognitive radio for flexible mobile multimedia communications," *IEEE Int. Workshop on Mobile Multimedia Communication*, Nov. 15–17, pp. 3–10, 1999.
- [2] B. Murmann, "A/D converter trends: Power dissipation, scaling and digitally assisted architectures," *IEEE CICC*, vol. 1, pp. 105–112, 2008.
- [3] R. H. Walden, "Analog-to-digital converter survey and analysis," *IEEE JSAC*, vol. 51, pp. 539–548, 1999.
- [4] X. Chen et al, "A Sub-Nyquist Rate Sampling Receiver Exploiting Compressive Sensing Signals", *IEEE TCAS-I*, pp. 1-14, 2010.
- [5] E. Candes, and T. Tao, "Decoding by linear programming," *IEEE Trans. on Inform. Theory*, vol. 51, pp.4203–4215, 2005.
- [6] F. Chen et al "Design and Analysis of a Hardware-Efficient Compressed Sensing Architecture for Data Compression in Wireless Sensors," *IEEE JSSC*, vol. 47, no.3, March 2012.

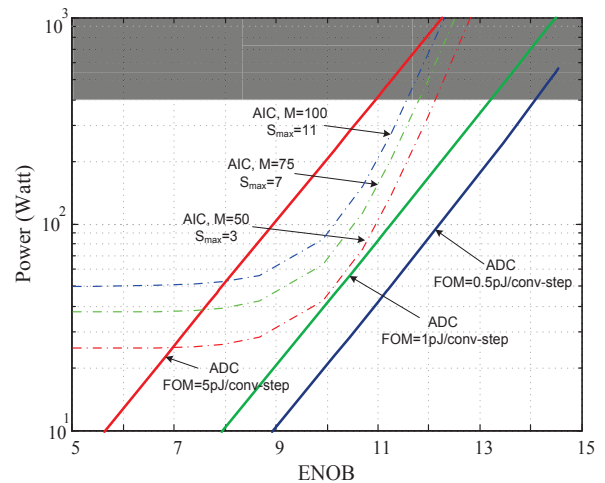


Figure 5: Power for the required ENOB, $G_A=1$.

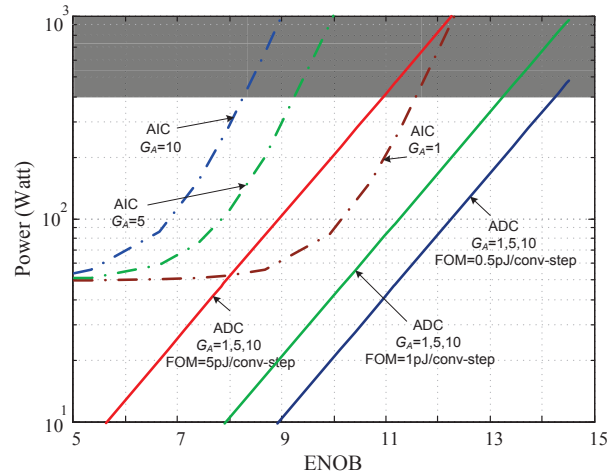


Figure 6: Power for the required ENOB and different receiver gain requirements, $M=100$.